MOBILITY CHARACTERISTICS AND CONTROL OF A SKID-STEERING MICRO-ROVER FOR PLANETARY EXPLORATION ON LOOSE SOIL

*Kenji Nagaoka[1], Kei Nakata[2], Shoya Higa[3], Kazuya Yoshida[4]

[1] *Tohoku University, Aoba 6-6-01, Aramaki, Aoba-ku, Sendai, Japan, E-mail: nagaoka@astro.mech.tohoku.ac.jp*
[2] *Tohoku University, Aoba 6-6-01, Aramaki, Aoba-ku, Sendai, Japan, E-mail: nakata@astro.mech.tohoku.ac.jp*
[3] *Tohoku University, Aoba 6-6-01, Aramaki, Aoba-ku, Sendai, Japan, E-mail: shoya@astro.mech.tohoku.ac.jp*
[4] *Tohoku University, Aoba 6-6-01, Aramaki, Aoba-ku, Sendai, Japan, E-mail: yoshida@astro.mech.tohoku.ac.jp*

ABSTRACT

This paper presents the mobility characteristics of a four-wheel skid-steering micro-rover in loose soil. The characteristics were experimentally investigated in terms of the effects of wheel grouser's height, rover's attitude, and the inclination angle of sloped terrain. The experimental results showed key relations between the roll angle and the forward traveling distance of the rover. On the basis of the relations, we developed two different steering controls with and without side-slip compensation for point-to-point slope traversal. We confirmed the validity of the control methods by comparative experiments. In addition, the energy consumption of the two steering control methods was analyzed, and its relationship to the steering maneuver was experimentally investigated. As a consequence, we found that the skid-steering rover consumed less energy when combined with spot-turning.

1 INTRODUCTION

Exploration rovers can perform in-situ scientific investigation on an extraterrestrial surface, such as on the Moon or Mars. Such robotic exploration technology has become increasingly important for challenging space missions. Likewise, low-cost space missions have received a lot of attention in recent years. Thus far, several light-weight micro-rover systems have been developed [1, 2] because an increase in the system weight directly increases launch costs. Hence, reductions in size and weight are required for a cost-effective rover mission. One feasible light-weight rover systems is a skid-steering system, which is used for typical tracked vehicles. This system can reduce the number of actuators needed, resulting in mechanical simplicity because a skid-steering rover does not need a specialized steering mechanism for turning a wheel. The rover can perform various steering maneuvers by different rotational velocities of the wheels on both sides of its main body.

A skid-steering system is often used for mobile robots. Some researchers have studied their dynamics modeling and control algorithms [3], which can be applied to the rover on an ideal flat surface. In actual lunar and planetary missions, however, the rover must travel over rough terrain covered with loose soil. Such terrain induces wheel slippage and sinkage [4, 5]. Wheel slippage in particular makes it difficult for the rover to follow the desired path. To facilitate wheeled mobility on loose soil, Ishigami et al. [6] modeled a rover's steering characteristics based on soil-wheel interaction mechanics, so-called terramechanics. They also achieved terramechanics-based slope traversal control in sand [7]. In this control method, the wheel's orientation was controlled to cancel the side-slip of the rover. This approach, however, targeted an all-wheel steering system.

This study focused on experimental investigation of the mobility characteristics of a skid-steering micro-rover on sloped sand. Based on the results, slope-traversal control methods are proposed. We implemented the methods in a four-wheel skid-steering micro-rover test bed and then evaluated them experimentally. This paper is organized as follows. In Section 2 and 3, the experimental mobility characteristics of the rover on flat and sloped sand, respectively, are presented. Section 4 shows the characteristic-based slope traversal controls and their evaluation. Section 5 summarizes the key results of this study.

2 MOBILITY CHARACTERISTICS ON FLAT SANDY TERRAIN

We first carried out experiments to understand the mobility characteristics of a skid-steering micro-rover on flat and loose soil. The experiments were performed using a four-wheel skid-steering test bed.

2.1 Experimental Equipment

In the experiments, we used MoonRaker-EM as a four-wheel skid-steering micro-rover test bed, which is an engineering model of a privately funded lunar micro-rover MoonRaker developed in our laboratory [8]. Figure 1 shows a schematic illustration of MoonRaker-EM and its wheel with parallel grousers. The rover weighs 8.0 kg including a camera unit, and its size is 0.3 m in width, 0.6 m in length, and 0.3 m in height. It also has an on-board

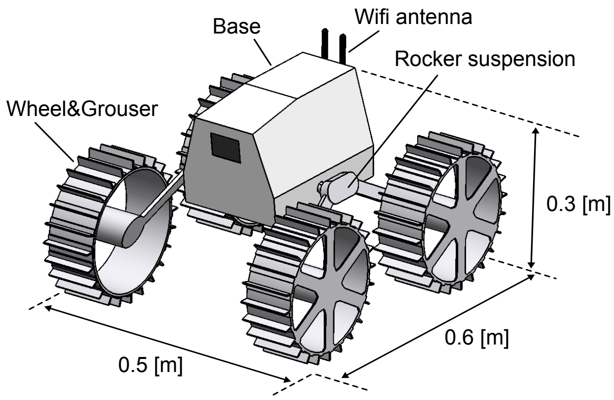

(a) Overview

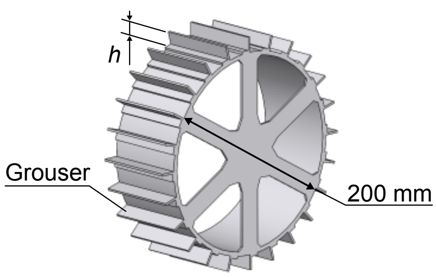

(b) Rigid wheel with parallel grousers

Figure 1 : Schematic illustration of MoonRaker-EM.

computer, and thus it can be remotely operated via wireless communication. We measured the rotational velocity of the output torque of each wheel by the embedded motor controllers during the experiments. In this study, the front and rear wheels on the same side were controlled have the same rotational velocity. The rover also has an embedded gyro sensor, and we measured the rover's relative attitude to the direction of gravity. To investigate the effect of the grousers, we used grouser of different heights h (10, 19, and 25 mm).

Figure 2 shows the overview of the experimental environment. The sand box is 1×2 m in size and filled with Toyoura standard sand. A motion capture camera system was set up around the sand box to obtain the accurate position and attitude of the test bed during the experiments. The sampling frequency of the cameras was 5 Hz. We calculated the center of balance position and the attitude of the rover based on the marker's position data.

2.2 Evaluation Index

As an evaluation index commonly used, we introduced the ratio of the rotational velocity of left- and right-side

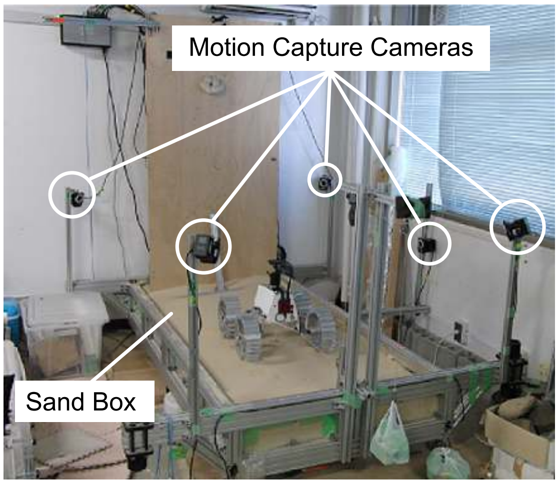

Figure 2 : Overview of sandy terrain in experiments.

wheels, γ, as follows:

$$\gamma = \begin{cases} \omega_r/\omega_l & \text{if } \omega_r \geq \omega_l \\ \omega_l/\omega_r & \text{otherwise} \end{cases} \tag{1}$$

where ω_l and ω_r are the rotation velocity of the left- and right-side wheels, respectively. The ratio also satisfies $-1 < \gamma < 1$.

A skid-steering rover has three maneuvering modes reflected in the γ value. When $\gamma = 1$, all the wheels rotate with the same velocity and the rover moves forward. When $\gamma = -1$, it performs a spot turn without changing its center of mass (C.O.M.) position, as shown in Figure 3a. When $-1 < \gamma < 1$, it moves along a circular trajectory, as shown in Figure 3b.

2.3 Linear Traction Experiment

To experimentally obtain the relationship between slip and drawbar pull, we carried out the traction experiments using the rover test bed, where traction load is applied to the rover on flat sandy terrain. Figure 4 illustrates the experimental configurations. The traction load was given by the pulleys as constant in a direction opposite the linear movement. The applied traction loads of 0, 5.3, 10.6, 15.9, 21.0, 26.1 and 31.1 N correspond to components of gravity force parallel to a slope surface with angles of 0, 5, 10, 15, 20, 25 and 30°, respectively. During the experiments, the rotation velocity of all wheels was set to 1 rpm.

In the traction experiments, we used two indexes to evaluate the rover's mobility characteristics. The first one is the wheel's slip ratio, s, which is defined as follows:

$$s = 1 - \frac{v_{rov}}{r_w \cdot \omega_w} \tag{2}$$

where v_{rov} is the rover's forward traveling velocity, r_w is the wheel radius, and ω_w is the wheel's rotational velocity.

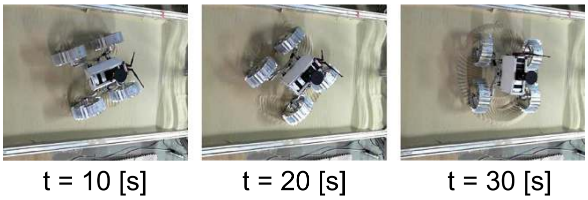

(a) $\gamma = -1.0$ *(where* $\omega_r \geq \omega_l$*)*

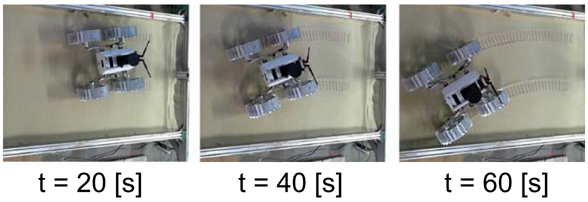

(b) $\gamma = 0.7$ *(where* $\omega_r \geq \omega_l$*)*

Figure 3 : Maneuvers of Moonraker-EM on flat sandy terrain.

In general, s takes a value between 0 and 1 for a tractive wheel,$s = 0$ is no slip between wheels and terrain, and $s = 1$ denotes wheels are stuck.

The second index is total energy consumption per unit distance traveled, f_{lin}, which is calculated as follows:

$$f_{lin} = \frac{W_{rov}}{v_{rov}} \tag{3}$$

where W_{rov} is the total work generated by the motors of the wheels. Smaller f_{lin} values indicate better energy efficiency.

Figure 5 shows the experimental result of relationship between f_{lin} and the traction load. The horizontal and vertical axes are the traction load and f_{lin}, respectively. When the traction load is smaller than 15 N, the grouser height, h, has no significant impact on f_{lin}. In contrast, when the traction load is over 15 N, the wheels with the higher h exhibits better energy efficiency. In addition, Figure 6 shows the experimental results of the relationship between s and f_{lin}. The horizontal and vertical axes are s and f_{lin}, respectively. Regardless of the difference in grouser height h, f_{lin} exponentially increases with increasing s. This result suggests that the slip ratio has more of an effect on energy efficiency than the grouser height.

2.4 Steering Experiment

A steering operation is required for a rover to avoid obstacles and follow a given path. To clarify the steering characteristics of the skid-steering rover, we carried out steering experiments. Here, we introduce he index f_{str}, which is defined as follows:

$$f_{lin} = \frac{W_{rov}}{\omega_{rov}} \tag{4}$$

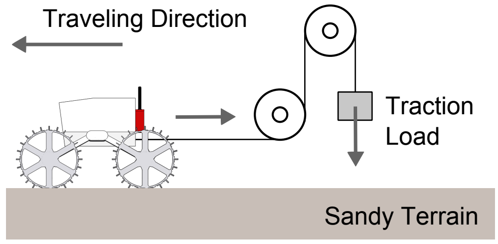

Figure 4 : Configuration of traction experiment.

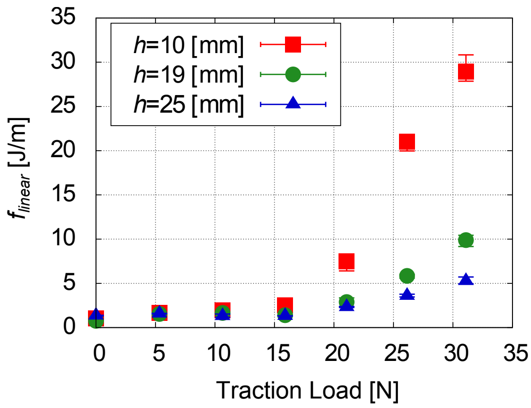

Figure 5 : Relationship between energy consumption and traction load.

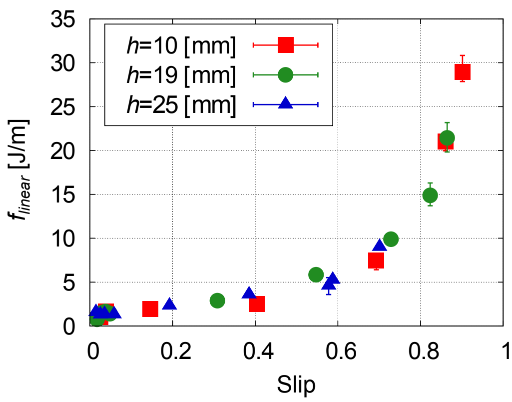

Figure 6 : Relationship between slip and energy efficiency.

where ω_{rov} is the spot-turning velocity of the rover. f_{str} is the spot-turning energy per unit angle change of rover attitude. A smaller f_{str} value denotes better energy efficiency.

Figure 7 shows the experimental results of the relationship between γ and f_{str}. A smaller γ value shows better energy efficiency. No significant difference was found for the different grouser heights.

2.5 Comparison of Steering Maneuvers

As described, a skid-steering rover can perform the three maneuvering modes by controlling γ. For point-to-point locomotion control, the skid-steering rover can perform

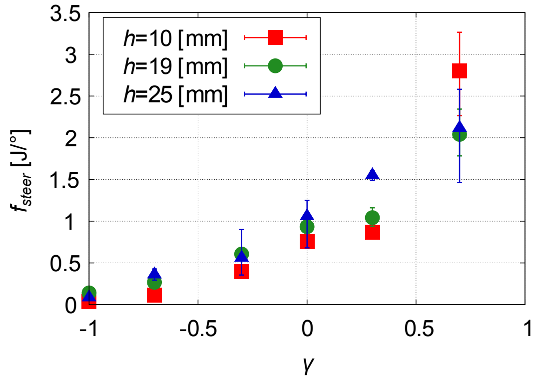

Figure 7 : Relationship between γ and steering energy efficiency.

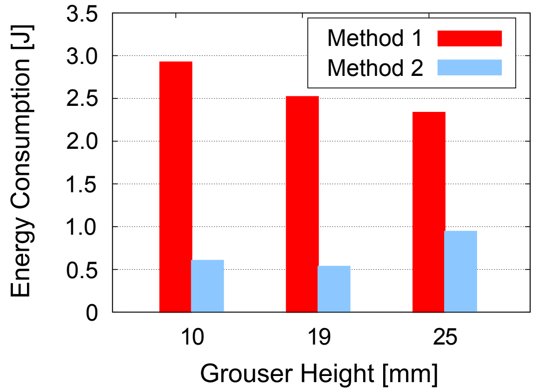

Figure 8 : Comparison of energy consumption of steering maneuvers in flat sand.

two different maneuvers. The first method (Method 1) is based on continuous circular maneuvers by continuous γ values: $-1 < \gamma < 1$. The second one (Method 2) is based on a combination of discrete γ values: spot-turning ($\gamma = -1$: spot-turning in order to head to the target point) and linear movement ($\gamma = 1$: moving linearly to the target point), which is the so-called bang-bang control.

The energy consumption of the two maneuvers is discussed. We obtained the energy consumption of Method 1, E_1, based on the experimental data. In the comparison, we used the results at $\gamma = 0.7$ for the point-to-point maneuver. E_1 is here defined as follows:

$$E_1 = \int \tau_w \cdot \omega_w \cdot dt \tag{5}$$

where ω_w is the rotational velocity of the wheel, which is ω_r or ω_l, and τ_w is the corresponding motor's output torque of the wheel.

For Method 2, we calculated the total energy consumption, E_2, based on f_{lin} and f_{str}. The equation we used for the second method is shown as follow:

$$E_2 = f_{str} \cdot \Delta\zeta + f_{lin} \cdot \Delta L \tag{6}$$

where $\Delta\zeta$ is an overall attitude change and ΔL is the distance between the initial and final points.

Figure 8 shows the experimental results of the energy consumption of the two methods. The results confirm that the maneuver combining spot-turning and linear movement is a more efficient method compared to the maneuver based on continuous γ. This advantage is independent of the grouser height.

3 MOBILITY CHARACTERISTICS ON SLOPED SANDY TERRAIN

We investigated the mobility characteristics of the skid-steering rover in slope traversal. Thus, we conducted traveling experiments to clarify the relationship between the slope angle, the grouser height, and motion trajectory. We simulated a slope by tilting the sand box, as shown in Figure 9. The coordinate system we defined is shown in Figure 10. The x axis is parallel to the slope traversal direction and the y axis is parallel to the slope upward direction. The origin of the coordinate system is the initial position of the rover. α is the inclination angle of the sand box. In these experiments, the linear movement conditions ($\gamma = 1$ and $\omega_r = \omega_l = 1$ [rpm]) were input.

3.1 Influence of Grouser Height

Two grousers of $h = 10$ and 25 mm were used for this evaluation. Figure 11a and Figure 11b show the results of the motion trajectory and heading angle ϕ (i.e., yaw angle), respectively. These confirm that the difference of h has little effect on the trajectory and yaw angle. In particular, the yaw angles were almost zero. These results show that it is difficult to prevent side-slip of the rover by changing the grouser height and that the rover's side-slip is produced without a change of its attitude.

3.2 Influence of Slope Angle

In the next experiments, we investigated the influence of the slope angle, α, on the motion trajectory, where we set $\alpha = 0$, 5, 10, and 15°. Figure 12 shows the resulting trajectories at each slope angle. All the trajectories are linear and their inclination increases with increasing α. Based on these results, we approximated the trajectories by a linear equation as follows:

$$y = K \cdot x \tag{7}$$

where K is constant.

We obtained K by a least squares method. Figure 13 shows the relationship between the obtained K values and the corresponding $\sin\alpha$ values. The results confirm that K is proportional to $\sin\alpha$. Hence, given a coefficient C, Eq. (7) can be re-written as follows:

$$y = C \sin\alpha \cdot x \tag{8}$$

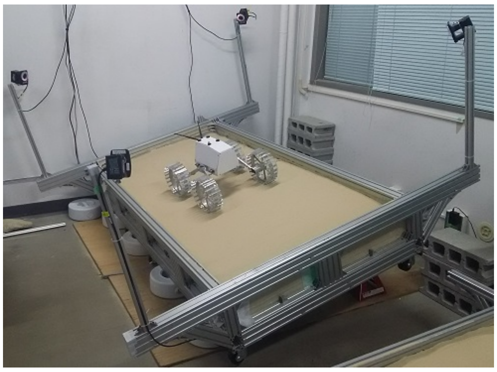

Figure 9 : Overview of slope traversal experiments.

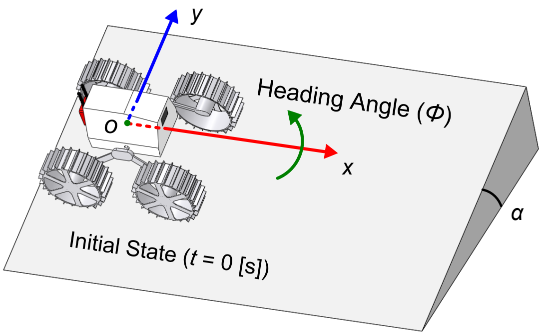

Figure 10 : Definition of inertial coordinate system for slope traversal experiments.

We finally determined $C = -0.33$ from Figure 13.

4 SLOPE TRAVERSAL CONTROL

Even on sloped sand, the rover is required to autonomously reach a target area while avoiding obstacles and critical slippage conditions. To meet such requirements, the rover must modify its wheel motion. For slope traversal, side-slip makes it difficult for the rover to follow a given path. In this section, we propose point-to-point slope traversal controls on loose soil based on the experimental mobility characteristics discussed in the previous sections.

4.1 Discrete Gamma Modulation Control (DGM Control)

As one control method, we propose discrete gamma modulation control (DGM control). Figure 14 shows the coordinate system $(\bar{x}, \bar{y})$ fixed on the rover's current C.O.M. position. $\bar{x}$ indicates the heading direction and $\bar{y}$ is normal to $\bar{x}$. θ is defined as the deviation angle from $\bar{x}$ to the directional vector of the target point $\mathbf{P}$. In DGM control, the rover moves forward with $\omega_r = \omega_r = 1$ [rpm] $(\gamma = 1)$ when θ is smaller than a threshold angle θ_{th}, where θ_{th} is

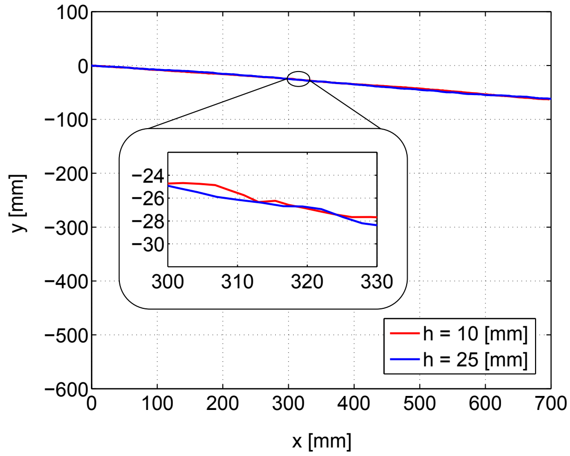

(a) Motion trajectory

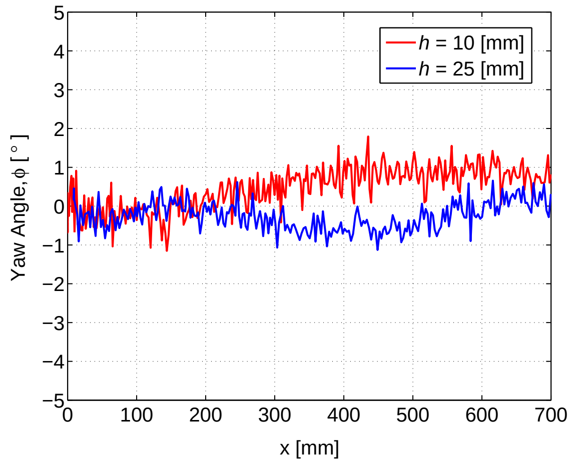

(b) Time history of ϕ

Figure 11 : Experimental results of slope traversal.

given as follows:

$$\theta_{th} = \theta_{thf} - \theta_{thi} \cdot \frac{|\mathbf{P}|}{|\mathbf{P_0}|} \tag{9}$$

where θ_{thf} and θ_{thi} are coefficients for the angle threshold and $|\mathbf{P_0}|$ is the initial distance to the target. In the experiments, θ_{thf} and θ_{thi} were set to 45° and 44°, respectively. When $\theta > \theta_{th}$, the rover performs the spot turn $(\gamma = -1)$ to decrease θ. The control input is selected as a discrete γ value, i.e., -1 or 1. This method is based on a feedback loop of the current attitude and C.O.M. position. Figure 15 shows a flowchart of the DGM control. Here, L_{th} is the tolerable range of the target point, which was set to 100 mm in subsequent experiments.

4.2 Side-Slip Compensation

Based on the experimental results in Section 3, we applied side-slip compensation to the DGM control. This compensates for the side-slip distance calculated from equa-

Figure 12 : Relationship between α and motion trajectory.

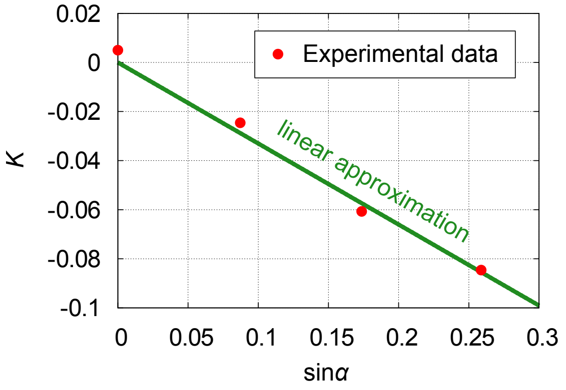

Figure 13 : Relationship between K and $\sin\alpha$*.*

tion Eq. (9) and modifies the target point upward. The position vector from the C.O.M. to the modified target point, $\mathbf{P}'$, is given as follows:

$$\mathbf{P}' = \mathbf{P} - C \sin\alpha \cdot |\mathbf{P}| \cdot \bar{\mathbf{y}} \tag{10}$$

where $\bar{\mathbf{y}}$ is a unit vector of $\bar{y}$.

Figure 16 shows a flowchart of the DGM control with the side-slip compensation. In every calculation cycle, P' is updated and the heading angle is modified based on θ'. Here, the slope angle α is measured by a gyro sensor inside the rover. This compensation utilizes the experimental characteristics as feedforward control based on the feedback data of the rover's position and attitude.

4.3 Evaluation of Side-Slip Compensation for DGM Control

The slope traversal experiments were carried out to evaluate the effectiveness of the DGM control with the side-slip compensation. The slope angle and target point were set $\alpha = 15$ [°] and $(x, y) = (1300 \text{ mm}, 0 \text{ mm})$, respectively. The grouser height of 10 mm was used in the experiments.

Figure 17 shows the resulting trajectories that we obtained from the evaluation experiments. The variation of the C.O.M. position in the y axis based on the control with compensation is smaller than that without compensation. The results confirm that the compensation law works effectively.

4.4 Continuous Gamma Modulation Control (CGM Control)

We also propose point-to-point slope traversal control as a continuous gamma modulation control, i.e., the control input is selected as $-1 < \gamma < 1$. In the first step, the radius r of the circular maneuver, which can go through both the current C.O.M. position and the target point, is calculated

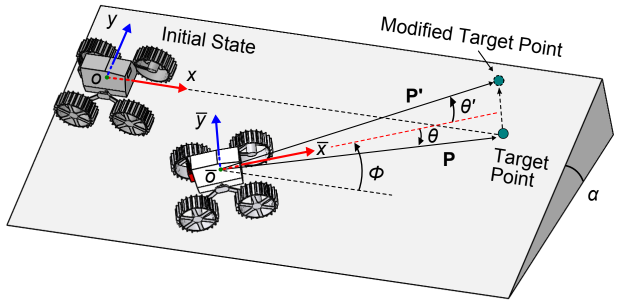

Figure 14 : Schematic of DGM control.

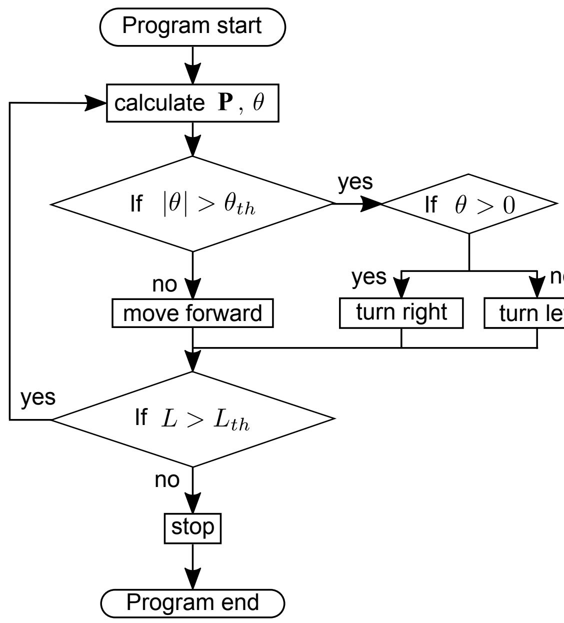

Figure 15 : Flowchart of DGM control system.

based on the rover's attitude and position. Figure 18 is a schematic of the CGM control. Given the center position of the circle locates on the same line of $\bar{y}$, we calculate r as follows:

$$r = \frac{1}{2} \cdot \frac{|\mathbf{P}|^2}{\mathbf{P} \cdot \bar{\mathbf{y}}} \tag{11}$$

On the basis of Eq. (11) and a bicycle model on a flat surface [9], we can compute γ as a control input to realize the desired radius as follows:

$$\gamma = \frac{-b_{rov} + 2r}{b_{rov} + 2r} \tag{12}$$

where b_{rov} is the distance between the right-side and left-side wheels, as shown in Figure 18. This method is also based on the same feedback loop with the DGM control.

4.5 Comparative Evaluation of CGM and DGM Control

A slope traversal experiment was performed to evaluate the DGM control. The experimental conditions were the

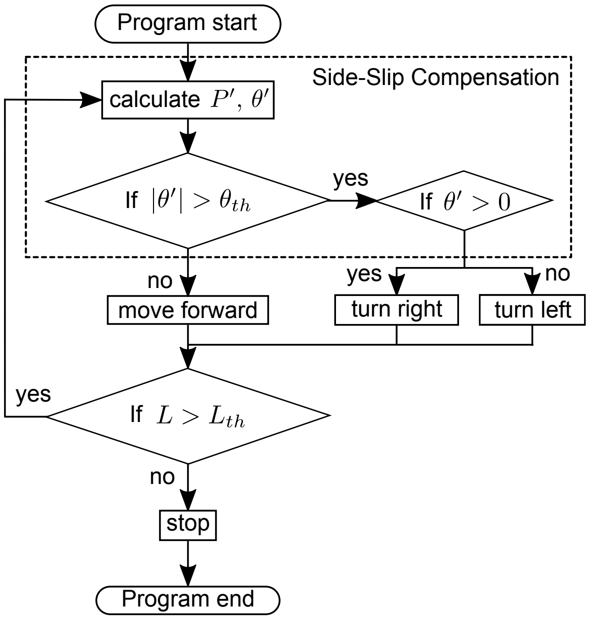

Figure 16 : Flowchart of DGM control system with side-slip compensation.

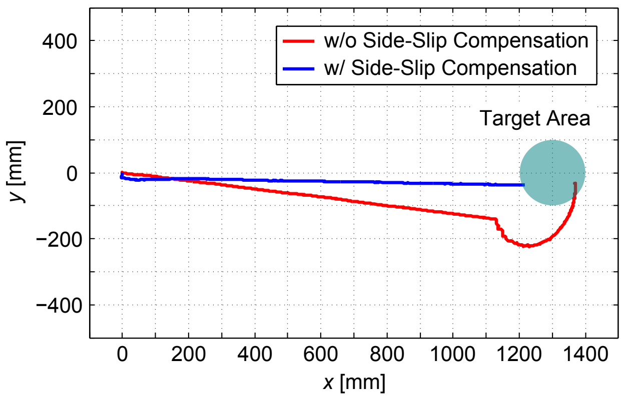

Figure 17 : Trajectories of slope traversal based on DGM control with and without side-slip compensation.

same as those used to evaluate the CGM control. In the DGM control, side-slip compensation was also implemented. Thus, the modified target point was given in its control loop.

Figure 19 shows the motion trajectories of the DGM and CGM controls for comparison. A snapshot of these experiments is shown in Figure 20. The CGM control's trajectory shows some variation of the C.O.M. position as compared to that of the DGM control

Furthermore, to compare the energy consumption of each system, we normalized the energy by the total traveling distance. The energy efficiency is defined as $\eta = E_t/L_t$, where E_t and L_t are the total energy consumption and the total traveling distance, respectively. Figure 21 shows the energy efficiency η of each control. The result-

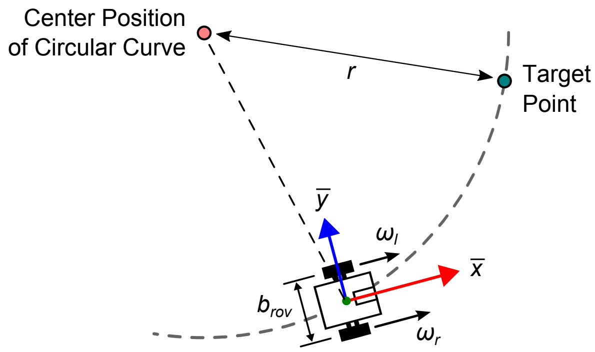

Figure 18 : Schematic of CGM control model.

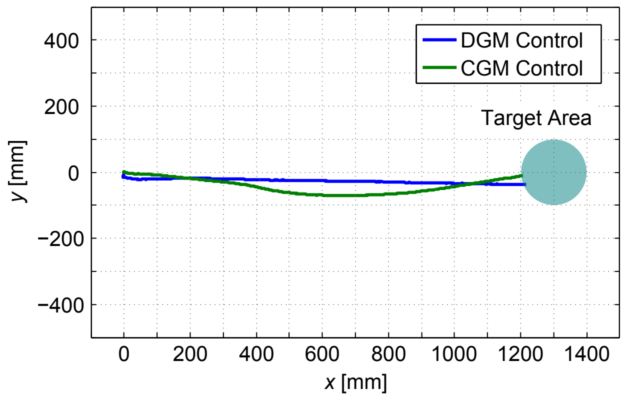

Figure 19 : Trajectories of slope traversal based on CGM and DGM controls with side-slip compensation.

ing values were averaged by three trials under the same conditions, and thus, the error bars are shown in Figure 21. From this comparison, we found that the DGM control is slightly more efficient than the CGM control as a slope traversal control method. This result indicates the same tendency as the steering experiments in flat sandy terrain.

5 CONCLUSION

In this paper, we discussed mobility characteristics and control methods of a four-wheel skid-steering micro-rover for slope traversal. From the traveling experiments on flat loose soil, it was found that the linear movement energy efficiency of the rover is dependent on the slip ratio of the wheels. We also calculated the energy consumption of two steering maneuvers and compared their energy consumption. The results confirmed that a more efficient steering maneuver can be achieved by combining spot-turning and linear movement. From the traveling experiments on sloped terrain, we clarified the key relationship between the slope angle, the grouser height, the rover attitude, and the rover's side-slip. As one of the key experimental characteristics, we introduced a relational equation for estimation of the side-slip. Based on these travel-

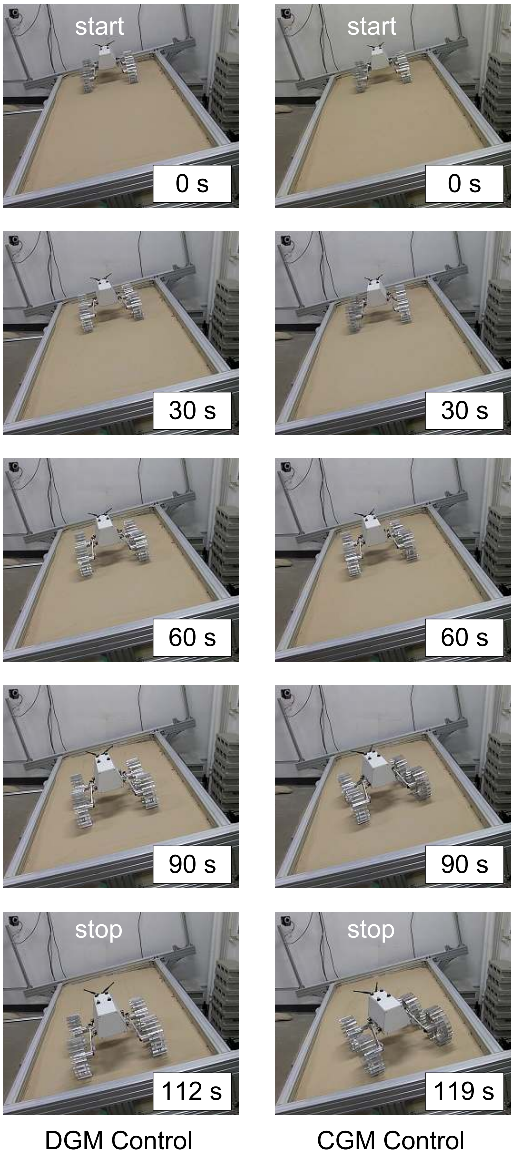

Figure 20 : Snapshots of CGM and DGM control experiments in sloped sand.

ing experiments on the slope, we proposed two point-to-point control methods, the CGM and DGM controls, and also side-slip compensation was applied to each control method. Comparing the motion trajectories of the CGM control with and without the side-slip compensation, the validity of the side-slip compensation was evaluated. The experimental comparison of the energy efficiency showed that the DGM control using discrete γ was more efficient than that using continuous γ. As a result, it is concluded that the skid-steering rover can achieve efficient maneuvers with less side-slip on sloped sandy terrain by combining spot-turning and linear movement.

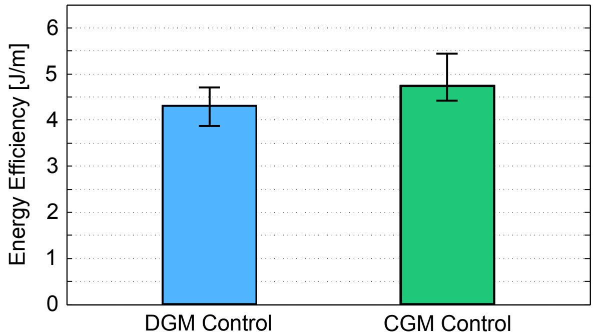

Figure 21 : Comparison of energy efficiency of CGM and DGM controls.

References

[1] M. Post, B. Quine, and R. Lee, "Beaver Micro-Rover Development for the Northern Light Mars Lander", *Proceedings of the 16th Bi-Annual Astronautics Conference of the Canadian Aeronautics and Space Institute*, 2012.

[2] A. Wedler et al., "LRU - Lightweight Rover Unit", *Proceedings of the 13th Symposium on Advanced Space Technologies in Robotics and Automation*, 2015.

[3] K. Kozłowski and D. Pazderski, "Modeling and Control of a 4-Wheel Skid-Steering Mobile Robot", *International Journal of Applied Mathematics and Computer Science*, vol. 14, no. 4, pp. 477–496, 2004.

[4] R. Irani, R. Bauer, and A. Warkentin, "A Dynamic Terramechanic Model for Small Lightweight Vehicles with Rigid Wheels and Grousers Operating in Sandy Soil", *Journal of Terramechanics*, vol. 48, no. 4, pp. 307–318, 2011.

[5] J. MacLennan, P. Jayakumar, C. Senatore, M. Wulfmeier, and K. Iagnemma, "Investigation of Stress and Failure in Granular Soils for Lightweight Robotic Vehicle Applications", *Proceedings of the 2012 NDIA Ground Vehicle Systems Engineering and Technology Symposium*, 2012.

[6] G. Ishigami, A. Miwa, K. Nagatani, and K. Yoshida, "Terramechanics-Based Model for Steering Maneuver of Planetary Exploration Rovers on Loose Soil", *Journal of Field Robotics*, vol. 24, no. 3, pp. 233–250, 2007.

[7] G. Ishigami, K. Nagatani, and K. Yoshida, "Path Following Control with Slip Compensation on Loose Soil for Exploration Rover", *Proceedings of the 2006 IEEE/RSJ International Conference on Intelligent Robots and Systems*, pp. 5552–5557, 2006.

[8] K. Yoshida, N. Britton, and J. Walker, "Development and Field Testing of Moonraker, a Four-Wheel Rover in Minimal Design", *Proceedings of the 12th International Symposium on Artificial Intelligence, Robotics and Automation in Space*, 2013.

[9] F. Solc and J. Sembera, "Kinetic Model of a Skid Steered Robot", *Proceedings of the 7th WSEAS International Conference on Signal Processing, Robotics Automation*, pp. 61–65, 2008.